Experimental evidence of two distinct charge carriers in underdoped cuprate superconductors

Samuele Sanna,[1,*] Francesco Coneri,[1] Americo Rigoldi,[1,2] Giorgio Concas,[2] and Roberto De Renzi[1]
[1]*Unità CNISM di Parma e Dipartimento di Fisica, I 43100 Parma, Italy*
[2]*Unità CNISM di Cagliari e Dipartimento di Fisica, I 09042 Monserrato (Ca), Italy*
(Received 7 May 2008; published 27 June 2008)

We present the results on heavily underdoped $Y_{1-x}Ca_xBa_2Cu_3O_{6+y}$, which provide the evidence that the doping mechanism (cation substitution or oxygen loading) directly determines whether the corresponding injected mobile holes contribute to superconductivity or only to high-temperature transport. We argue that this hole tagging is a signature of the complexities of single-hole doping in Mott insulators, and it calls for a subtler description of the correlated bands than the usual one. We also map in great detail the underdoped superconducting phase diagram T_c vs hole doping, which shows that the total number of mobile holes is not the driving parameter for superconductivity.

DOI: 10.1103/PhysRevB.77.224511 PACS number(s): 74.25.Fy, 74.72.−h, 71.30.+h, 76.75.+i

I. INTRODUCTION

The behavior of a hole in the cuprate doped Mott-Hubbard insulator is often described in a *universal* picture where, above some critical concentration, it forms the Zhang-Rice singlet[1] in a single correlated-band scheme. However, structural and compositional details of each specific compound do influence the fine grain behavior. Growing evidence that more than one band is needed comes from $Ca_xLa_{1.25}Ba_{1.75-x}Cu_3O_{6+y}$, where two distinct charge fluids have been reported[2] by nuclear quadrupole resonance (NQR). At optimum doping tunneling spectroscopy directly detects[3] two CuO_2 gaps in $Y_{1-x}Ca_xBa_2Cu_3O_{6+y}$, and muon spin rotation (μSR) provides additional supporting evidence[4] in the case of $La_{2-x}Sr_xCuO_4$. In the underdoped regime early nuclear magnetic resonance (NMR) (Refs. 5 and 6) and recent magnetotransport[7] results demonstrate that besides band carriers giving rise to superconductivity, additional thermally activated doped holes exist. The activation energy, proportional to x^{-1}, has been shown to scale with relevant angle-resolved photoemission spectroscopy (ARPES) Fermi-arc features, and it has been linked directly to the pseudogap.[8] Further details, such as the presence of Fermi pockets from high field quantum oscillations,[9] call for a subtler band structure implementation.[10] Activated holes are also indirectly detected through the magnetic order parameter reduction measured with NQR and μSR (Refs. 11 and 12). It seems that at least two bands[13] are needed to correctly describe real cuprates.

This scenario indicates that two distinct electronic components are invoked in different context, throughout the underdoped to optimal regime of the cuprates and in different materials as well. It is an open question whether all of these claims indicate an intrinsic properties of any realistic model of the active $Cu(2)O_2$ layer or they are evidence of material specific features.

One of the details that distinguishes real-world cuprates from the idealized models is the doping mechanism, which can proceed via heterovalent cation substitution, as in the case of $La_{2-x}Sr_xCuO_4$, or through oxygen filling in a building block more removed from the active layer, as in the case of $YBa_2Cu_3O_{6+y}$. The specific mechanism may well bear indirect effects on the relevant electronic structure, besides that of charge transfer, since it influences distortion, hence orbital mixing on Cu and the composition of the Cu bands.

For this reason we chose to investigate a compound where the two doping mechanisms coexist: in $Y_{1-x}Ca_xBa_2Cu_3O_{6+y}$, charge doping is provided both by the heterovalent $Ca^{+2} \rightarrow Y^{+3}$ substitution, controlled by x, and by the interstitial oxygen content, y, in the Cu(1)O chain layer, yielding a total hole concentration $h=h_{Ca}+h_O$ transferred to the active layers. We could thus directly show that the two contributions behave very differently with respect to room temperature normal properties and superconductivity.

II. EXPERIMENTAL METHODS

Polycrystalline samples were prepared by a topotactic technique, which consists in the oxygen equilibration of stoichiometric quantities of the two end members, tightly packed in sealed vessels.[14] Low temperature annealing yields high quality homogeneous samples with an absolute error of $\delta x = \pm 0.02$ in oxygen content per formula unit (reduced to ± 0.01 after recalibrating end member of different batches). Besides this determination, absolute oxygen content is cross-checked by iodometric titration, thermogravimetry on each sample, and selected neutron Rietveld refinements. Ca content is checked by x-ray and neutron Rietveld refinements. Reported error bars are the global errors from this procedure. Transition temperatures correspond to the linear extrapolation of the 90–10% diamagnetic drop of the susceptibility, measured in a field of $\mu_0 H=0.2$ mT. These data agree within quoted uncertainties with resistive determinations (and μSR, when available). The width of the interval where the resistance drops from 90–10% of the onset value is typically 6 K for $y \leq 0.4$, like for Ca free pellets and large single crystals (see Ref. 15 and references therein). The μSR experiment were performed on the MUSR spectrometer of the ISIS pulsed muon facility in the transverse field (TF) geometry,[16] where an external magnetic field $\boldsymbol{H}$ is applied perpendicular to the initial muon spin $\boldsymbol{S}_\mu$ polarization.

III. RESULTS

The inset in Fig. 1 shows the progressive reduction of T_c vs x in the $y \simeq 0.9$ end members (our starting polycrystals, reacted and annealed in oxygen atmosphere), witnessing the

 ©2008 The American Physical Society

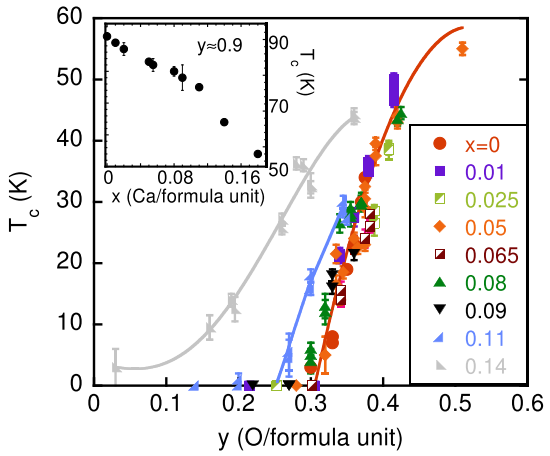

FIG. 1. (Color online) Superconducting transition temperatures T_c of $Y_{1-x}Ca_xBa_2Cu_3O_{6+y}$ samples vs oxygen concentration for the whole set of samples: The $x \leq 0.09$ data fall on the same line (curves are guides to the eye). Inset: transitions T_c detected by SQUID magnetization vs calcium concentration, for the fully oxygenated, $y \approx 0.9$ samples. The reduction of T_c with increasing x is the signature of overdoping due to Ca substitution.

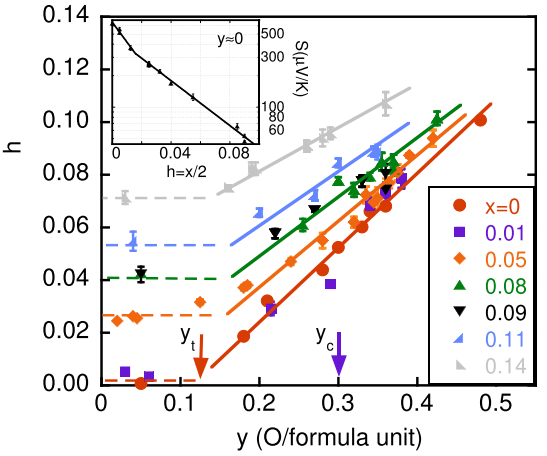

FIG. 2. (Color online) Total hole content of $Y_{1-x}Ca_xBa_2Cu_3O_{6+y}$ samples h, obtained from thermopower vs oxygen content y, for different Ca families. Inset: calibration of holes h per $Cu(2)O_2$ layer from thermopower S at $T=290$ K for the fully reduced samples.

double doping mechanism.[17,18] The superconducting transition measured by superconducting quantum interference device (SQUID) magnetometry is progressively reduced from the maximum $T_c=92$ K at $x=0$ (optimal doping), as Ca substitution injects additional holes: both h_{Ca} and h_O contribute to superconductivity, driving the samples into the overdoped region. The smooth linear dependence of $T_c(x)$ of the inset in Fig. 1 also guarantees an effective Ca-Y substitution in the whole explored range.

When we tune the oxygen content of the same samples to low doping, close to the metal-insulator boundary, we find a markedly different behavior. Figure 1 displays the critical temperature T_c versus oxygen content y for series of samples at fixed calcium content, $0 \leq x \leq 0.14$. T_c falls on the same curve for $x \leq 0.09$, and superconductivity appears at the same critical oxygen concentration, $y_c=0.30$. This implies that Ca-doped holes, which are transferred into the CuO_2 layers disrupting antiferromagnetism (AF) with the same efficiency of Sr in $La_{2-x}Sr_xCuO_4$ (Ref. 19), do not have any appreciable influence on T_c in our underdoped ($x \leq 0.09$) samples.

Why are holes transferred by Ca and O not additive for superconductivity in the low doping regime? The different cationic radii ($R_{Ca^{+2}}/R_{Y^{+3}} \approx 1.1$) may trivially alter oxygen order in the Cu(1)O chains, reducing their charge transfer efficiency. This is the case, e.g., for substantial Y substitutions,[20] where the formation of chains takes place at much larger oxygen content. An independent assessment of the hole content is required to rule out this effect. The Seebeck coefficient is an independent measure of the mobile carrier content, since an exponential dependence of S vs h is observed in $YBa_2Cu_3O_{6+y}$ in a large range of doping.[17,18] We systematically measured the value of S at room temperature (RT), $T=290$ K, calibrating the dependence on the fully reduced compounds, $y \approx 0$ samples equivalent to $h_O=0$, by assuming an average hole content per Cu plane $h=h_{Ca}=x/2$. We identify two regions as in a previous work,[17] and our best fit to $S(h)=\alpha \exp(-\beta h)$, shown in the inset of Fig. 2, yields values of $\alpha=480$ μV/K and $\beta=25$ for $h>0.016$ and $\alpha=650$ μV/K and $\beta=44$ for $h<0.016$.

Figure 2 shows the h values obtained for all our $Y_{1-x}Ca_xBa_2Cu_3O_{6+y}$ samples ($0 \leq x \leq 0.14$) by comparing their RT Seebeck coefficient S with the calibration curve of the inset in Fig. 2, under the assumption[17,18] of nearly equal mobilities for the two types of holes, h_O and h_{Ca} (Ref. 21). Notice that in the entire range of oxygen content explored in this paper, $0.05 \leq y \leq 0.42$, the Cu(1)O chains do not produce[22] a normal metal contribution to the thermopower, hence the measured hole density is located in the CuO_2 layers.

Figure 2 shows the well known fact that oxygen does not contribute to hole transfer up to $y_t \approx 0.12-0.15$ (red arrow), since below this threshold O concentration, only locally charge-neutral Cu(1)OCu(1) dimers are formed,[23] while above y_t hole doping increases almost linearly with y, as oxygen ions start forming negatively charged trimers. This is true whatever the calcium content, which proves that the oxygen doping mechanism remains nearly the same with a minor dependence of y_t on x (dashed line in Fig. 2). The samples ($x=0$, 0.05, and 0.08), which collapse on the same curve in Fig. 1, still show a large difference in their total RT mobile hole content $h(y)$ at the critical oxygen concentration $y_c=0.3$ (blue arrow in Fig. 2) for the appearance of superconductivity.[24]

We also plot in Fig. 3 the reduced critical temperature $T_c/T_{c,max}$ versus h ($T_{c,max}$ is the maximum transition temperature of each calcium series at optimum doping[22]), showing beyond doubt that the onset of superconductivity does not fall on the same curve as a function of the total hole content h. Each series of samples at constant x follows its own curve, contradicting the suggested *universal* parabolic relation[25] between T_c and h, which is not the driving parameter in cuprate superconductivity as it is often assumed. A similar situation is evidenced by NMR (Ref. 2) in $Ca_xLa_{1.25}Ba_{1.75-x}Cu_3O_{6+y}$, where the NQR interaction shows that not all doped carriers contribute to the superconducting order parameter.

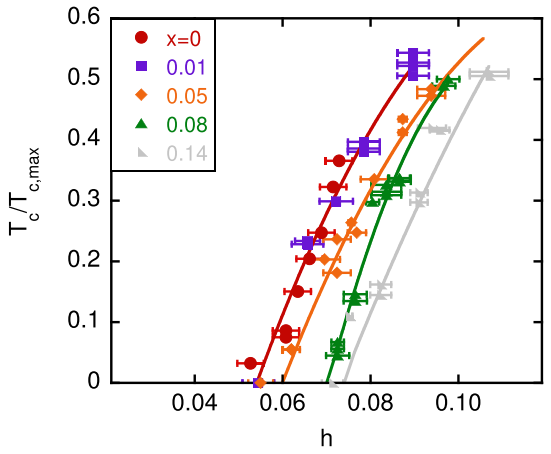

FIG. 3. (Color online) Scaling of transition temperatures with RT total holes: $T_c/T_{c,\max}$ does not scale with the total hole content h. Here $T_{c,\max}$=93, 92, 91, 89, and 87 K, respectively for x=0, 0.01, 0.05, 0.08, and 0.14 (from Ref. 22).

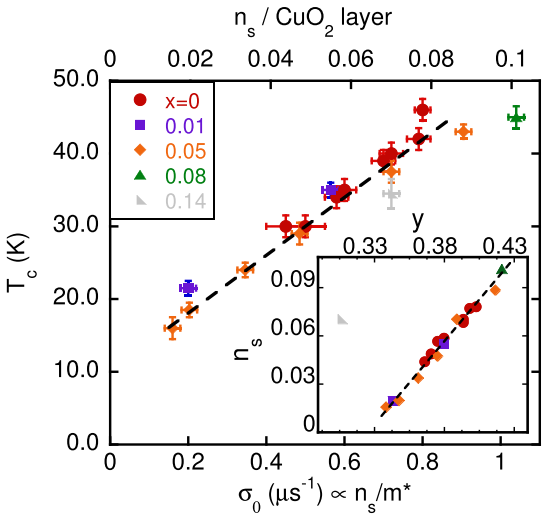

FIG. 4. (Color online) Scaling of transition temperatures with pair density: T_c does scale with the μSR linewidth σ_0, proportional to the supercarrier density n_s. Inset: supercarrier density vs oxygen content. The samples for $0<x<0.08$ collapse on the same line, which yields to $n_s \propto y$ (see text), i.e., only the oxygen hole fraction h_O contribute to the supercarrier density for low calcium content.

The observed shift of $T_c(h,x)$ to higher h for $x>0$ (Fig. 3) could remind the pair-breaking effect of Cu-substituted Zn (Ref. 26). We can however dismiss pair breaking as its major cause for Ca, since unlike Zn (the strongest known scatterer in the unitary limit), Ca is removed from the CuO_2 layers, and it produces a very small T_c reduction at optimal doping, $\Delta T_{co}=-4$ K for $x=0.08$ (Ref. 22) a factor 20 less than Zn (Ref. 26). If ΔT_{co} for Ca is entirely attributed to pair breaking, the worst case reduction at large underdoping (unitary limit, see Fig. 3 in Ref. 26) is only $\approx 1.5\Delta T_{co}=-6$ K, whereas our Fig. 3 corresponds to a much larger $\Delta T_c=-27$ K at $h=0.07$, between $x=0.08$ and $x=0$.

The supercarrier pair density n_s was directly determined by TF μSR experiments. We measured two series with $x=0$, $x=0.05$, and variable y, plus two further samples ($x=0.08$, $y=0.43$ and $x=0.14$, $y=0.30$). Field cooling the samples in $\mu_0 H=0.022$ T a flux lattice is formed, whose field inhomogeneity determines a depolarization rate of the muon spin precession $\sigma(T)$, proportional to the inverse square of the London penetration depth λ_L, hence to the supercarrier density n_s (Ref. 27): $\sigma(T) \propto n_s(T)/m^*$, where m^* is the electron effective mass. All samples with $y<0.4$ display a coexistence of magnetism, below the freezing temperature T_f, and superconductivity, below T_c. The supercarrier density at zero temperature $\sigma_0=\sigma(T=0)$ must be obtained by extrapolating the data between these two transitions, as in Refs. 15 and 28.

The dependence of T_c on $\sigma_0 \propto n_s/m^*$ shown in Fig. 4, approaches the characteristic linear *Uemura-plot* behavior.[29] The upper axis of the plot represents the supercarrier density n_s per CuO_2 plane, calculated in the clean limit approximation as $n_s[\text{hole/CuO}_2] \approx 97\,500 \cdot \sigma_0$, obtained by combining the relation $\sigma_0=7.58 \cdot 10^{-8} \lambda_L^{-2}$ in international system of units (SI) (Ref. 30) with $\lambda_L^{-2}=\mu_0 e^2 n_s/m^*$. We assume a doping independent value of the effective mass $m^*=3m_e$ (Ref. 31). The plot of supercarrier density vs oxygen content $n_s(y)$, displayed in the inset of Fig. 4, shows that all samples with calcium content $0<x<0.08$ collapse on the same line, i.e., the dependence of n_s on y is linear. Since also holes injected by oxygen scale with y, $h_O \propto y-y_t$ (Fig. 2), the two linear relations imply that only the fraction of holes injected by oxygen h_O contributes to the supercarrier density for low calcium content. Incidentally, Fig. 4 shows a shift from the original *Uemura plot* toward lower σ_0, a feature already noticed[32,33] and currently under debate. This shift is opposite to what is observed when metallic chains are present for $y \geq 0.8$ (Ref. 34)

IV. DISCUSSION AND CONCLUSIONS

Our results show that in heavily underdoped compounds, additional holes transferred from Ca participate to the RT thermopower (Fig. 2) with $h_{Ca} \propto x$. Figure 4 however shows that their contribution disappears from coherent conduction at low temperatures: whereas holes transferred from Cu(1)O chains contribute both to RT transport (above the threshold concentration $y_t \approx 0.15$, $h_O \propto y-y_t$) and to superconducting properties [above the critical concentration $y_c=0.3$, $n_s \propto \sigma_0 \propto Tc \approx k(y-y_c)$], the Ca holes do not take part in the latter. Since pair breaking does not account for this effect, Ca-doped holes behave *as if* they were thermally activated.

Notice that our results do not simply detect a reduction of coherent vs RT conduction densities: they furthermore indicate a mechanism of hole tagging, since the hole origin (i.e., whether they are transferred from Ca or from O) determines their behavior. Since Ca transfers charges directly into the CuO_2 layer, very efficiently quenching AF order, and Fig. 2 shows that charge transfer from chain oxygen is almost independent of Ca content, we must conclude that two kinds of hole coexist in the CuO_2 layers. Hence the specific semiconducting behavior that we witness must be intrinsic to the nature of charge excitations in doped Mott insulators (see Ref. 35 and references therein).

It looks particularly difficult to reconcile this tagging with

simple one-band Hubbard models.[1] *Vice versa* the well known CuO_2 plane buckling does bring into play two Cu e_g bands, and the different ionic radii in cation-substituted cuprates imply a local Jahn-Teller distortion, which couples to both of them. This is likely to be an essential ingredient for any realistic model of actual cation-substituted cuprates. This implies that one or both of the two types of carriers may be spatially correlated on the nanoscopic scale to the distortion introduced locally by the substituted cation, a feature which may be related to the observed tagging.

We further argue that our results have a consequence on the broader understanding of cuprates. The activated transport that we indirectly deduce in $Y_{1-x}Ca_xBa_2Cu_3O_{6+y}$ is a generic feature of the extremely underdoped regime in compounds where cation substitution is the only doping mechanism. For instance Hall effect measurements[7] identify similar activated mobile holes in $La_{2-x}Sr_xCuO_4$. Importantly, it was pointed out that the activation energy is proportional to x^{-1} and that this matches also quantitatively the pseudogap features[8] determined by ARPES. Recent theoretical calculations[13] show that a two-band Hubbard model may yield two distinct excitations that fit this pictures, providing a nontrivial origin for the activated behavior. A straightforward conjecture is that *for all* cuprates the two features, namely, the activated behavior and the pseudogap excitations are two sides of the same coin. If we assume this conjecture to be valid for the $Y_{1-x}Ca_xBa_2Cu_3O_{6+y}$ system as well, our results suggest that pseudogap excitations are specifically related to Ca-tagged doping.

ACKNOWLEDGMENTS

We acknowledge the support of PRIN06, "Search for critical parameters in high T_c cuprates," partial support of PRIN05, "Coexistence of magnetism and metallicity in high-Tc superconducting oxides," NMI3-Access and the staff of the ISIS facility (MUSR and GEM-XPRESS). We thank G. Calestani and L. Righi for their help in diffraction refinements and also G. Guidi, G. Allodi, A. Keren, A. Damascelli, and V. Fiorentini for fruitful discussions.

*Samuele.Sanna@fis.unipr.it

[1] F. C. Zhang and T. M. Rice, Phys. Rev. B **37**, 3759 (1988).
[2] A. Keren, A. Kanigel, and G. Bazalitsky, Phys. Rev. B **74**, 172506 (2006).
[3] J. H. Ngai, W. A. Atkinson, and J. Y. T. Wei, Phys. Rev. Lett. **98**, 177003 (2007).
[4] R. Khasanov, A. Shengelaya, A. Maisuradze, F. La Mattina, A. Bussmann-Holder, H. Keller, and K. A. Muller, Phys. Rev. Lett. **98**, 057007 (2007).
[5] A. Rigamonti, F. Borsa, M. Corti, T. Rega, and F. Waldner, in *Early and Recent Aspects of Superconductivity*, edited by G. Bednorz and K. A. Mueller (Springer, Berlin, 1990), pp. 441–466.
[6] A. Rigamonti, F. Borsa, and P. Carretta, Rep. Prog. Phys. **61**, 1367 (1998).
[7] S. Ono, S. Komiya, and Y. Ando, Phys. Rev. B **75**, 024515 (2007).
[8] L. P. Gor'kov and G. B. Teitel'baum, Phys. Rev. Lett. **97**, 247003 (2006).
[9] N. Doiron-Leyraud, C. Proust, D. LeBoeuf, J. Levallois, J.-B. Bonnemaison, R. Liang, D. Bonn, W. Hardy, and L. Taillefer, Nature (London) **447**, 565 (2007).
[10] I. S. Elfimov, G. A. Sawatzky, and A. Damascelli, Phys. Rev. B **77**, 060504(R) (2008).
[11] F. Borsa, *et al.*, Phys. Rev. B **52**, 7334 (1995).
[12] S. Sanna, G. Allodi, and R. De Renzi, Solid State Commun. **126**, 85 (2003).
[13] A. O. Sboychakov, K. I. Kugel, and A. L. Rakhmanov, Phys. Rev. B **76**, 195113 (2007).
[14] P. Manca, S. Sanna, G. Calestani, A. Migliori, S. Lapinskas, and E. E. Tornau, Phys. Rev. B **63**, 134512 (2001).
[15] S. Sanna, G. Allodi, G. Concas, A. D. Hillier, and R. De Renzi, Phys. Rev. Lett. **93**, 207001 (2004).
[16] A. Schenck, *Muon Spin Rotation Spectroscopy* (Adam Hilger, Bristol, 1986).
[17] S. D. Obertelli, J. R. Cooper, and J. L. Tallon, Phys. Rev. B **46**, 14928 (1992).
[18] T. Honma, P. H. Hor, H. H. Hsieh, and M. Tanimoto, Phys. Rev. B **70**, 214517 (2004).
[19] C. Niedermayer, C. Bernhard, T. Blasius, A. Golnik, A. Moodenbaugh, and J. I. Budnick, Phys. Rev. Lett. **80**, 3843 (1998).
[20] H. Lutgemeier, S. Schmenn, P. Meuffels, O. Storz, R. Schollhorn, C. Niedermayer, I. Heinmaa, and Y. Baikov, Physica C **267**, 191 (1996).
[21] The calibration curve in the inset in Fig. 2 is a phenomenological fit, and our conclusions are independent of its details. In particular Fig. 2 is self-similar if one assumes a uniform transfer rate $h=kx$, with a different k coefficient.
[22] C. Bernhard and J. L. Tallon, Phys. Rev. B **54**, 10201 (1996).
[23] G. V. Uimin, V. F. Gantmakher, A. M. Neminsky, L. A. Novomlinsky, D. V. Shovkun, and P. Brull, Physica C **192**, 481 (1992).
[24] A slight reduction of the $h(y)$ slope with increasing x above y_t, has more probably to do with different mobilities of h_O and h_{Ca}, rather than with the above mentioned trimer formation threshold.
[25] M. R. Presland, J. L. Tallon, R. G. Buckley, R. S. Liu, and N. E. Flower, Physica C **176**, 95 (1991).
[26] J. L. Tallon, C. Bernhard, G. V. M. Williams, and J. W. Loram, Phys. Rev. Lett. **79**, 5294 (1997).
[27] B. Pümpin *et al.*, Phys. Rev. B **42**, 8019 (1990).
[28] G. Allodi, S. Sanna, G. Concas, R. Caciuffo, and R. De Renzi, Physica B **374-375**, 221 (2006).
[29] Y. J. Uemura, *et al.*, Phys. Rev. Lett. **62**, 2317 (1989).
[30] W. Barford and J. Gunn, Physica C **156**, 515 (1988).
[31] W. J. Padilla, Y. S. Lee, M. Dumm, G. Blumberg, S. Ono, K. Segawa, S. Komiya, Y. Ando, and D. N. Basov, Phys. Rev. B **72**, 060511(R) (2005).
[32] A. Kanigel, A. Keren, A. Knizhnik, and O. Shafir, Phys. Rev. B **71**, 224511 (2005).
[33] D. M. Broun, W. A. Huttema, P. J. Turner, S. Özcan, B. Morgan, R. Liang, W. N. Hardy, and D. A. Bonn, Phys. Rev. Lett. **99**, 237003 (2007).
[34] C. Bernhard, *et al.*, Phys. Rev. B **52**, 10488 (1995).
[35] P. A. Lee, N. Nagaosa, and X.-G. Wen, Rev. Mod. Phys. **78**, 17 (2006).